Journal of Electron Spectroscopy and Related Phenomena 172 (2009) 95–103

Contents lists available at ScienceDirect

Journal of Electron Spectroscopy and Related Phenomena

journal homepage: www.elsevier.com/locate/elspec

Modification of PET surfaces with self-assembled monolayers of organosilane precursors

Ali E. Ozcam[a], Kirill Efimenko[a], Cherno Jaye[b], Richard J. Spontak[a,c], Daniel A. Fischer[b], Jan Genzer[a,*]

[a] Department of Chemical & Biomolecular Engineering, North Carolina State University, Raleigh, NC 27695-7905, United States
[b] Ceramics Division, National Institute of Standards and Technology, Gaithersburg, MD 20899, United States
[c] Department of Materials Science & Engineering, North Carolina State University, Raleigh, NC 27695-7907, United States

ARTICLE INFO

Article history:
Available online 27 March 2009

Keywords:
Poly(ethylene terephthalate) (PET)
Ultraviolet/ozone (UVO)
Polymer surface modification
SAM
NEXAFS

ABSTRACT

We report on a facile, robust and rapid method by which poly(ethylene terephthalate) (PET) surfaces can be chemically modified while avoiding chemical degradation. Specifically, we demonstrate that brief exposure of PET surfaces to ultraviolet/ozone (UVO) generates a large surface concentration of hydrophilic moieties that serve as points of chemical attachment, thereby facilitating subsequent chemisorption of organosilane precursors. The feasibility of this methodology is tested by decorating UVO-modified PET surfaces with semifluorinated organosilane (SFOS) molecules, which serve to alter the surface energy of PET without compromising its bulk characteristics. The physico-chemical properties of the SFOS layers attached to PET are studied with a palette of experimental probes, including near-edge X-ray absorption fine structure (NEXAFS) spectroscopy, X-ray photoelectron spectroscopy (XPS), contact angle, atomic force microscopy (AFM), and ellipsometry. Experimental results indicate that ≈2 min of UVO treatment is optimal for covering PET with dense self-assembled monolayers (SAMs) of SFOS. Longer UVO treatment times contaminate and correspondingly roughen PET surfaces with low-molecular-weight organic compounds (LMWOCs) generated from degradation of the topmost PET material. As a consequence, SFOS SAMs attached to the LMWOC layer readily wash off from UVO-treated PET.

1. Introduction

Since its discovery in the 1940s [1], poly(ethylene terephthalate) (PET) has become one of the most important and widely used thermoplastic polymers. Its high tensile and impact strength, adequate CO_2 retention, chemical resistance, optical clarity, processability, and design flexibility have expedited commercial use of PET in a wide variety of applications including, but not limited to, high-value/low-cost consumables (*i.e.*, textile fibers, beverage bottles, jars, tire cords, audio tapes, and photographic film). It is also an ideal candidate for futuristic applications such as a substrate material for flexible electronic circuits. Among all thermoplastics and engineering polymers, PET has experienced the largest growth rate – its overall worldwide consumption reaching 9.1 million tons in 2003 – and is expected to hit nearly double this production level by 2010 [2].

Like most organic polymers, PET does not possess good adhesion and wetting properties because of its inherently low surface energy. For some applications it is desirable to alter the PET surface character, either chemically or physically, without compromising its bulk properties [3]. In the past, several efforts have reported on modifying the surface of PET by using chemical treatment (*e.g.*, hydrolysis [4–7], reduction [7–9], aminolysis [5,8–10], and glycolysis [7]) and physical modification (*e.g.*, plasma [11,12], ultraviolet/ozone [12–16], flame [12], corona treatments [12,17,18], electrical discharge [19], ion beam bombardment [20], laser treatment [21], surface physical interpenetrating network formation [22], and surface graft polymerization after activation of the PET surface [3,10]). Since most of these surface modification techniques purposefully or inadvertently involve polymer degradation, careful selection of experimental conditions is imperative to the successful surface modification of PET without degrading the bulk polymer and its desirable property attributes.

Ultraviolet/ozone (UVO) treatment has traditionally been used as an expedient technique to remove organic impurities from semiconductor surfaces [23]. This method of treatment involves a photosensitized oxidation process wherein the molecules of the treated material are excited and/or dissociated by the absorption of short-wavelength UV radiation. The excited molecules then inter-

* Corresponding author at: Department of Chemical & Biomolecular Engineering, North Carolina State University, 911 Partners Way, PO Box 7905, Raleigh, NC 27695-7905, United States. Tel.: +1 919 515 2069.
E-mail address: Jan_Genzer@ncsu.edu (J. Genzer).

0368-2048/$ – see front matter © 2009 Elsevier B.V. All rights reserved.
doi:10.1016/j.elspec.2009.03.012

act with atomic oxygen simultaneously generated as molecular oxygen and ozone are dissociated by UV radiation at wavelengths of 184.9 and 253.7 nm, respectively. Therefore, when a specimen is exposed to both wavelengths, molecular oxygen is continuously converted into ozone that subsequently breaks into reactive atomic oxygen. Concurrently, the 253.7 nm radiation is absorbed by most hydrocarbons and the organic products of this excitation react intensely with atomic oxygen to form simpler volatile molecules (*i.e.*, CO_2), which desorb from the surface. Over the past few years, several papers have reported on the use of UVO treatment to modify the surfaces of polyethylene [24,25], polypropylene [13,14,26], PET [13–16], polystyrene [15], poly(dimethylsiloxane) [27] and poly(etherether-ketone) [25]. While the exact surface composition after UVO treatment varies from polymer to polymer, the concentration of hydrophilic groups, such as –COOH or –OH, at or near the surface generally increases dramatically for all polymers. In addition to these surface-anchored, high-surface-energy moieties and some volatile components (*i.e.*, CO_2), UVO treatment may "leave behind" a residual layer composed of hydrophilic low-molecular-weight organic compounds (LMWOCs). These LMWOCs represent non-volatile components that can be removed by washing the surface with an appropriate solvent, including water [13,14].

Modification of PET surfaces by UVO treatment has been investigated previously by Walzak et al. [12–14] and Bradley et al. [15,16], who explored the effect of UVO treatment time on PET surface energy [13–16], chemical composition [13–16], topography [15,16], and aging [13]. They report an increase in the wettability of PET surfaces accompanied by an increase in surface oxygen concentration and roughening with increasing UVO treatment time. In addition, they have demonstrated increases in contact angle and carbon concentration after washing the UVO-treated PET specimens with water and/or aging the sample. These increases are attributed to removal of LMWOCs formed during UVO treatment and migration of hydrophilic moieties to the bulk of the sample. In this work, we modify the surface of PET by UVO treatment as a preparatory step that enables more general chemical tailorability of PET surfaces. Specifically, UVO-modified PET surfaces are shown to exhibit a large number of hydrophilic moieties that can serve as attachment points for organosilane molecules (OS). We demonstrate here the applicability of this technique by attaching self-assembled monolayers (SAMs) of semifluorinated OS (SFOS) precursors to UVO-treated PET substrates and report on the physicochemical characteristics of SFOS SAMs attached to the surface of PET films.

2. Methods

2.1. Film preparation

Bulk PET films were obtained either by melt-pressing flakes or using untreated Mylar-DL films donated by DuPont-Teijin Films. The average surface roughness of the films, as measured by atomic force microscopy (AFM), was 2.0 ± 0.2 nm. These films were rinsed with deionized water (DIW) and methanol and then extracted with hexane for at least 8 h. After extraction the films were dried under vacuum and kept in a desiccator under reduced pressure until modification. Thin PET films were prepared by dissolving PET flakes in *o*-chlorophenol at a concentration of 3% (w/w) and subsequently spin-casting onto flat silica substrates that were previously rinsed with methanol and DIW. After deposition, the PET films were exposed to UVO. These films were used to monitor the relative changes in surface properties and film thickness as functions of UVO treatment time.

2.2. Ultraviolet/ozone treatment

The UVO treatment of PET surfaces was performed in a commercial UVO chamber (Jelight Company, Inc., model 42).[1] The standard fused quartz lamp, which, according to the manufacturer, emits about 65% of the total radiation at 184.9 nm and has an output of 28 mW/cm^2 at a distance 6 mm away from the source, was used in this study. The PET films were placed onto glass slides, which were subsequently inserted into the UVO cleaner at a distance of about 5 mm from the UV source and exposed to UVO radiation from one side only for predetermined periods of time.

2.3. Semifluorinated self-assembled monolayer formation

1H,1H,2H,2H-Perfluorodecyl trichlorosilane (tF8H2), supplied by Alfa-Aesar and used as-received, was employed to form semifluorinated SAMs on the UVO-treated PET films prior to specimen sonication. The tF8H2 and fluorinated oil were mixed in a 1:5 ratio (w/w), and a small amount of this mixture was placed on the bottom of a Petri dish. After virgin and UVO-treated PET and silica substrates were taped to the Petri dish lid, the whole system was enclosed so that the samples hung face-down on the Petri dish $\approx$1 cm away from the tF8H2/oil mixture. Upon exposure for 15 min at ambient conditions, the lid was removed and the samples were first washed thoroughly with absolute ethanol to remove any physisorbed tF8H2 molecules and then dried with nitrogen.

2.4. Surface characterization methods

Contact-angle measurements were performed via the sessile drop technique with DIW (the resistance was >15 MΩ cm) using a Ramé-Hart contact angle goniometer (Model 100-00) equipped with a CCD camera. Images were analyzed with the Ramé-Hart Imaging 2001 software. Static contact angles (S-CAs) were determined upon placement of an 8 μL droplet of DIW on the specimen surface. To measure the advancing and receding contact angles (A-CAs and R-CAs, respectively), a probe droplet was added (2 μL, DIW advancing) or removed (4 μL DIW, receding) and analyzed. Contact angles were measured on three to five independent spots on each sample and the results were averaged. The corresponding contact angle hysteresis (CAH), defined as the difference between the A-CA and R-CA, was likewise evaluated as a measure of the chemical and structural homogeneity of the surface probed. The surface topography of virgin and modified PET samples was examined using an Asylum Research MFP-3D AFM instrument in AC mode using Olympus AC-240 silicon cantilevers. Specimens were mounted with superglue to sample disks to ensure sample immobilization during imaging. Caution was exercised to keep the tip in repulsive mode in the phase channel during imaging. The root-mean-square (RMS) surface roughness was calculated from height images using the MFP-3D software. The thicknesses of spun-cast PET films were measured with a variable-angle spectroscopic ellipsometer (VASE) manufactured by J.A. Woollam Co. Ellipsometry measures the difference in the polarization state between the light beams incident onto and reflected from the surface, thus providing information about the dielectric properties and thickness of the film. The thickness of the films was evaluated using a single layer Cauchy model (Si/SiO_x/PET, index of refraction of PET was $n = 1.5751$ at 630 nm) before and after UVO treatment, as well as after sonication, rinsing with DIW and drying with nitrogen gas. During this latter procedure, LMWOC debris is removed from

[1] Identification of a commercial product is made only to facilitate reproducibility and to adequately describe procedure. In no case does it imply endorsement by NIST or imply that it is necessarily the best product for the procedure.

the PET-UVO specimens. Unless otherwise specified, ellipsometric data were collected at an incidence angle of 70° to the surface normal at wavelengths ranging from 400 to 1100 nm in 10 nm increments.

The surface chemical composition of UVO-modified PET specimens was determined with a Kratos Axis Ultra DLD X-ray photoelectron spectroscopy (XPS) instrument using monochromated Al Kα radiation with charge neutralization. Survey and high-resolution spectra were collected with pass energies of 80 and 20 eV, respectively, by using both electrostatic and magnetic lenses. Elemental chemical compositions were determined from spectral regression using Vision and CasaXPS software. Near-edge X-ray absorption fine structure (NEXAFS) spectroscopy above the carbon, oxygen and fluorine K-edges was also used to examine the composition and molecular orientation of the tF8H2 monolayers and the surface chemistry of the UVO-modified PET samples. The NEXAFS experiments were conducted at the NIST/Dow Soft X-ray Materials Characterization Facility of the National Synchrotron Light Source (NSLS) at Brookhaven National Laboratory. This spectroscopic method involves the resonant soft X-ray excitation of a K-shell electron to an unoccupied low-lying anti-bonding molecular orbital of σ symmetry (σ*) or π symmetry (π*) [28]. The initial state K-shell excitation endows NEXAFS with its elemental specificity, while the final-state unoccupied molecular orbitals provide NEXAFS with its bonding or chemical selectivity. Measurement of the partial electron yield (PEY) intensity of NEXAFS spectral features thus allows identification of chemical bonds and determination of their relative population densities on a sample surface (the probing depth is ≈3–4 nm subsurface). In addition, because the incident X-ray is linearly polarized, collection of NEXAFS spectra at various sample/X-ray beam orientations can yield information regarding the molecular orientation of molecules present on the surface. For this purpose, NEXAFS spectra have been collected at $\theta = 20$, 50 and 90°, where θ is the angle between the sample normal and the polarization vector of the X-ray beam.

3. Results and discussion

As mentioned earlier, atomic oxygen generated during UVO treatment reacts rapidly with various chemical functionalities present on the material surface and breaks polymer chains into smaller molecular fragments. While volatile species (*i.e.*, CO_2) escape readily during this process, heavier LMWOC fractions remain as deposits on the polymer surface and can be removed by water rinsing or sonication. Sample thickness changes associated with UVO treatment and washing are monitored in this study by ellipsometry. In Fig. 1, the thickness change upon UVO treatment (Fig. 1a) and the water sonication step (Fig. 1b) are plotted as functions of UVO treatment time. From these data, it is apparent that the amount of material removed during UVO exposure increases steadily at a rate of ≈4.5 nm/min. The quantity of LMWOCs removed by sonication increases with increasing UVO treatment time and saturates at around 12 min, corresponding to a thickness of ≈22 nm. These results reveal that the overall rate of PET removal is ≈6 nm/min (Fig. 1c).

The S-CA of the UVO-treated PET surface has also been monitored before and after removal of the water-soluble LMWOCs to discern the effect of residue removal on the surface energy of the film. The data in the top plot of Fig. 2 display the S-CA prior to and after sonication as a function of UVO treatment time. In both instances, the S-CA values decrease with increasing UVO treatment time, confirming UVO-induced oxidation of the surface and an increase in the population of hydrophilic groups probed by the DIW droplet. For a given UVO treatment time, the S-CA values after removal of the LMWOC layer are slightly higher relative to the S-CA prior to the sonication step. It is important to recognize that the S-CA after water sonication appears to reach a plateau around ≈40° after ≈5 min of UVO treatment. The increase in the S-CA, attributed to the removal of a large fraction of residual hydrophilic molecules from the surface by sonication, indicates that the surface functionalities remaining on the surface are not as hydrophilic as the LMWOC debris.

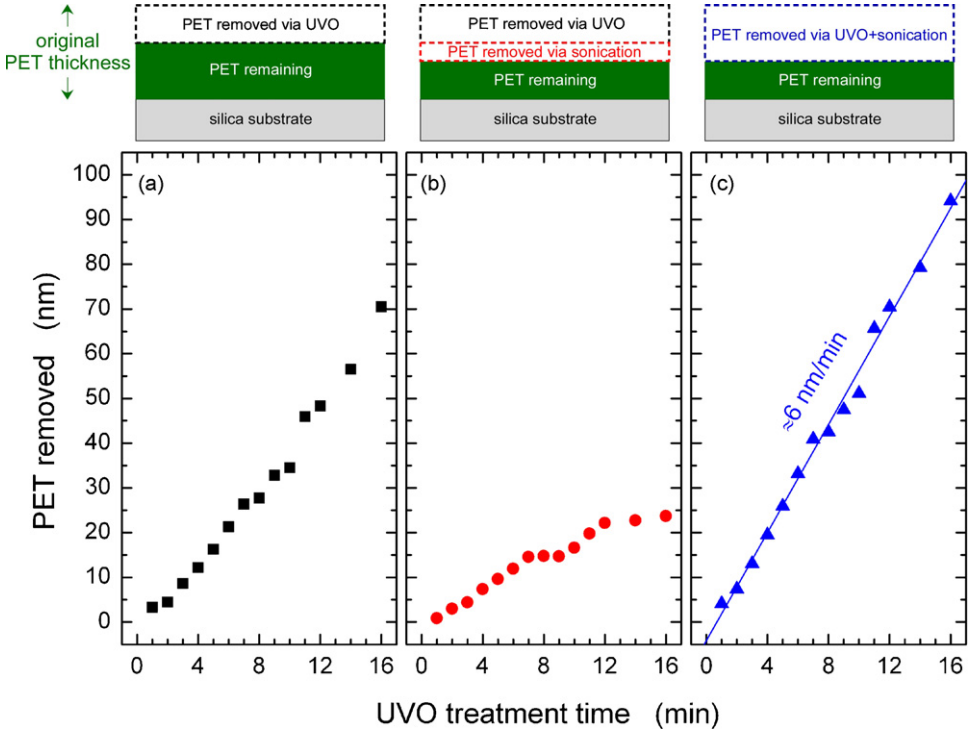

Fig. 1. Thickness of PET at various stages of surface treatment. The original thickness decreases with increasing UVO treatment time (a) and decreases further after subsequent sonication (b). The total thickness of PET removed from the sample is shown in (c). The line in part (c) denotes the overall PET removal rate (≈6 nm/min).

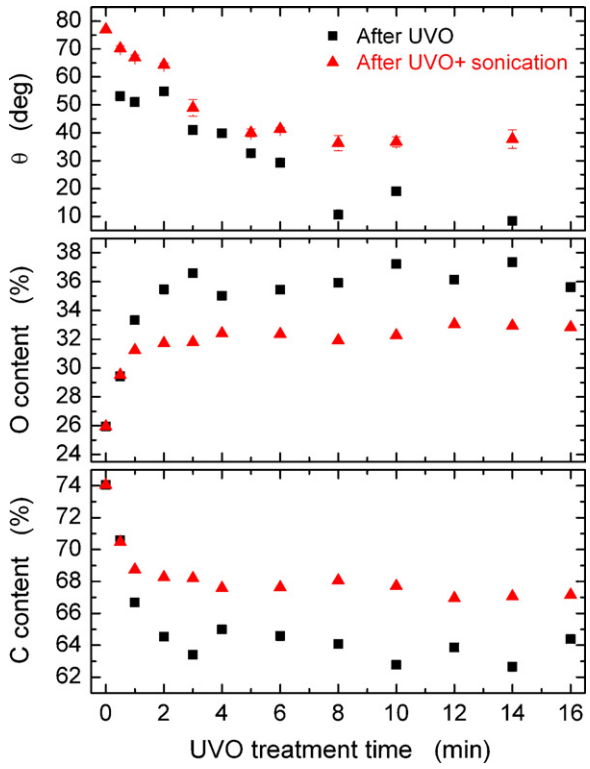

Fig. 2. Static water contact angle (top), oxygen content (middle), and carbon content (bottom) as functions of UVO treatment time immediately after UVO treatment (black squares) and after UVO followed by sonication (red triangles). The contact angle was measured by contact-angle goniometry, and the elemental compositions were determined by XPS. (For interpretation of the references to color in this figure legend, the reader is referred to the web version of the article.)

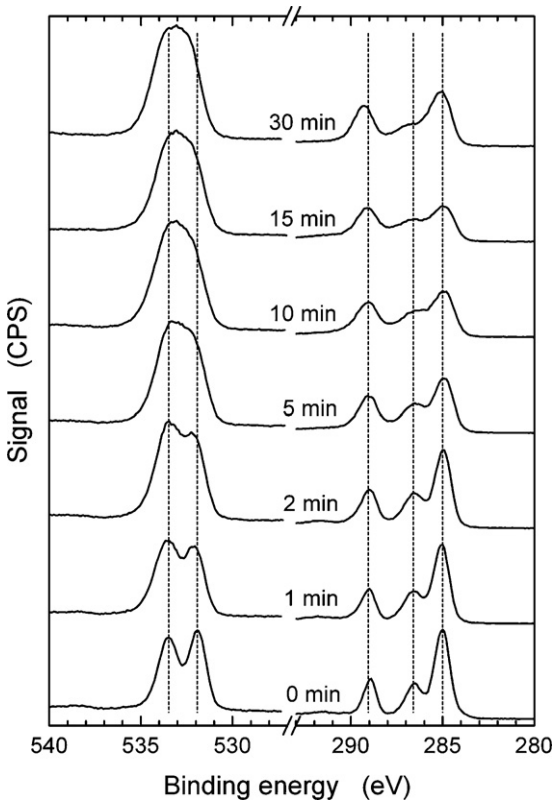

Fig. 3. High-resolution XPS spectra of PET samples in the oxygen (before break) and carbon (after break) regions after treated with UVO for various times.

The surface chemical composition evolution of PET films is evident from the XPS measurements presented as a function of UVO treatment time in Fig. 2. Here, the elemental concentrations of oxygen and carbon are provided in the middle and bottom plots, respectively. Removal of LMWOCs promotes a decrease in the concentration of atomic oxygen and a corresponding increase in the atomic carbon concentration relative to values measured on PET-UVO surfaces. The concentrations of atomic oxygen and carbon increase and decrease, respectively, with increasing UVO treatment time, and they both reach a plateau after ≈3–5 min. Note that this time agrees favorably with the onset of the plateau in the S-CA data (*cf.* Fig. 2 top). It is not surprising that the XPS and S-CA data exhibit similar trends, since both techniques probe the upper-most regions of a sample: ≈10 nm (XPS) and ≈0.5 nm (S-CA). In addition to the S-CA and XPS measurements, we have also monitored the variation in surface chemical composition in PET-UVO samples by NEXAFS spectroscopy. Though not shown, the NEXAFS K-edge jump results also agree qualitatively with the XPS and S-CA trends presented in Fig. 2.

Chemical changes due to oxidation of the PET surface are elucidated by analyzing high-resolution XPS 1 s scans for carbon and oxygen. Fig. 3 shows the relative intensities of the major component peaks in both the O1s (525–540 eV) and C1s (275–294 eV) regions. Visual inspection of the XPS spectra reveals that an increase in UVO exposure time causes the peaks to broaden and the peak intensities in the O1s region to increase, while those in the C1s region to decrease. These results indicate that the oxygen content in the sample increases whereas that of carbon decreases (on a relative basis). The component peaks located at 285.0, 286.6, 287.9, and 289.0 eV correspond to the C–C/C–H, C–O/C–O–C, O–C–O/C═O, and O═C–O signals, respectively [29–32]. Intensity variations in these characteristic "XPS fingerprints" with increasing UVO treatment time are displayed in Fig. 4 for samples before and after sonication. For example, the peak located at 289.0 eV, the characteristic binding energy for carbon in carboxyl groups, increases in intensity relative to the peak located at 285.0 eV, assigned to C–C/C–H groups. This observation establishes that the percentage of lower binding energy component from high-resolution oxygen spectra (data not shown for C═O: 532.8 eV and C–O: 533.6–544.3 eV) increases. The binding energy of carbon in acid and ester functionalities is slightly different [29,31,32]. From the data presented in Fig. 4, the percentage of C–C/C–H bonds decreases initially from ≈50% down to ≈40% and does not change further during the course of longer UVO treatment. However, removal of the LMWOC layer via sonication increases the amount of C–C/C–H bonds compared to those in the samples prior to sonication. The population of O═C–O bonds increases and reaches a plateau region after ≈4 min of UVO exposure for both sonicated and un-sonicated specimens. Conversely, the opposite trend is evident for the O═C–O bonds relative to C–C/C–H bonds, *i.e.*, after washing-off the LMWOC layer, the population of O═C–O bonds decreases in comparison to samples before sonication. The concentration of C–O bonds increases for the first 2 min and then levels off. Washing-off the LMWOC layer has the same effect on the concentration of C–O bonds. According to the data provided in Fig. 4, UVO treatment of PET introduces carboxylic acids and hydroxyl groups on the PET surface. Surface-bound –OH groups are crucial to the success of this study, since they will serve as attachment points for organosilane precursors, as described below.

The surface morphology of PET after UVO treatment for 0, 2, 8 and 30 min has been examined by AFM. Fig. 5 shows representative AFM images acquired from samples before (left) and after (right) washing the UVO-treated PET films. For comparison, an AFM image of the parent PET substrate is included in Fig. 5a. From images such as these, it is evident that the surface topography

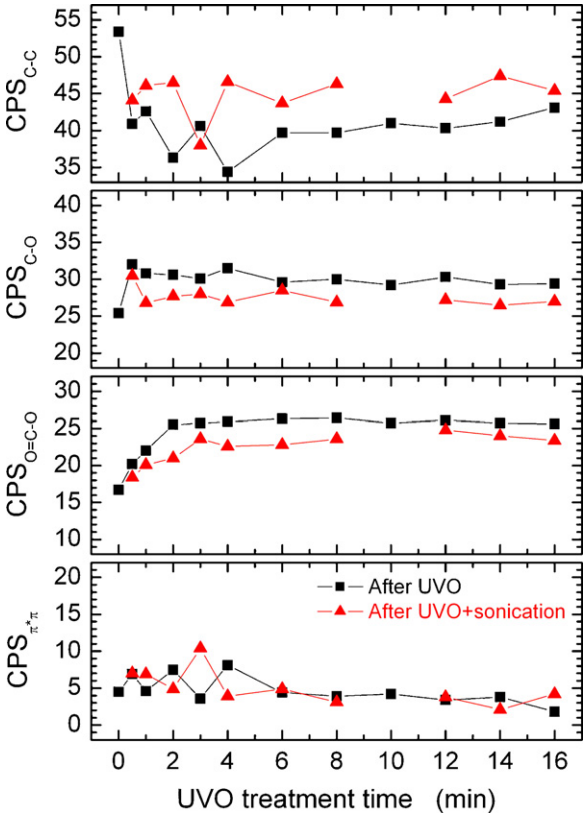

Fig. 4. Atomic percentages of various chemical functionalities present in the PET-UVO specimens, determined by XPS, as a function of UVO treatment time before (black squares) and after (red triangles) sonication. The lines are meant to guide the eye. (For interpretation of the references to color in this figure legend, the reader is referred to the web version of the article.)

of the films does not change significantly in the first ≈2 min of UVO treatment. After ≈8 min, however, UVO treatment appreciably alters the surface topography. Specifically, discrete, spheroidal grains measuring ≈82 ± 4 nm in diameter become apparent. The size of these grains increases with increasing UVO exposure time, reaching ≈113 ± 7 nm in diameter after 30 min. After removing the LMWOC layer, the size of the grains decreases to ≈66 ± 2 and ≈81 ± 6 nm at 8 and 30 min, respectively. We note that similar results are obtained by scanning electron microscopy (images not shown here).

The presence of surface-bound hydrophilic functionalities introduced during the UVO treatment of PET can be utilized to attach reactive OS precursors, which are known to chemisorb to (predominantly) –OH groups on the surface [33,34]. As a proof of concept, we use SFOS, which is based on a trichlorosilane head group, as molecules that react rapidly with surface-bound –OH groups even at ambient temperatures [35]. The SFOS SAMs have been deposited from vapor on top of the PET-UVO samples, as detailed in Section 2. The properties of the PET-UVO/tF8H2 samples have been characterized by a variety of analytical methods, as described in detail below. As mentioned earlier, the removal of physisorbed tF8H2 molecules is performed using absolute ethanol to be more efficient than DIW and likewise prevent hydrolysis of unreacted OS from the surface. Independent ellipsometry experiments have been conducted to compare the removal efficacy of the LMWOC layer from UVO-treated PET after washing with ethanol and sonicating in DIW. This comparative study has verified that absolute ethanol constitutes a better solvent for removing LMWOCs from the PET-UVO surfaces than DIW.

In Fig. 6 the S-CA of PET-UVO/tF8H2 samples after sonication is presented as a function of UVO treatment time. For comparison we also provide data from tF8H2 SAMs formed on top of a silicon wafer covered with a thin layer of silica (SiO_x/tF8H2). Whereas the S-CA for the SiO_x/tF8H2 samples remains at ≈115° for all UVO times and agrees well with previously reported results [35], the S-CA values of tF8H2-treated PET are consistently lower than those measured on SiO_x/tF8H2. Furthermore, excluding the datum point for untreated PET, the S-CA values generally decrease with increasing UVO treatment time. This reduction is due to the removal of LMWOC components that have reacted with tF8H2 during the ethanol rinsing step. By comparing the S-CA values of PET-UVO (*cf.* Fig. 2) and PET-UVO/tF8H2 (*cf.* Fig. 6) samples at long UVO treatment times, we conclude that some tF8H2 SAMs remain on the PET-UVO surface even after washing. The CAH for PET-UVO/tF8H2 samples ranges between 10° and 15°, which are not very different from the CAH measured in regard to SiO_x/tF8H2 SAMs (7–11°). This finding is interesting and somehow uneasy to reconcile, since it implies that the surfaces of the PET-UVO/tF8H2 specimens remain relatively uniform. This implication and other issues related to the effect of LMWOC layer removal on SFOS SAMs are currently being investigated and will be reported in the future.

The population and molecular orientation of the tF8H2 molecules comprising the SAMs on top of the PET-UVO substrates have been interrogated by NEXAFS spectroscopy. In Fig. 7, PEY NEXAFS spectra collected from PET-UVO/tF8H2 samples at the fluorine K-edge at $\theta = 50°$ are shown. At this geometry, representing the so-called "magic angle," the PEY NEXAFS intensities are independent of molecular orientation and hence provide a convenient measure of molecular concentration in the specimens [28]. These and subsequent PEY NEXAFS spectra have been normalized so that the intensity in the "pre-edge" region (photon energies <685 eV) is set equal to zero. The value of the so-called "edge-jump," defined as the difference between the "post-edge" (photon energies >700 eV) and the "pre-edge," represents a convenient relative measure of the concentration of fluorine in the sample. From the data displayed in Fig. 7, the highest fluorine content measured is present in the PET-UVO/tF8H2 sample prepared by exposing PET films to UVO for 2 min. The fluorine level decreases with increasing UVO treatment time due to the removal of the LMWOC layer, along with the tF8H2 SAM attached to it. This result agrees well with the trend in the CA data discussed previously (*cf.* Fig. 6). The density of the tF8H2 molecules comprising the surface SAM constitutes another important parameter to consider because it determines the stability of the SAMs on top of the LMWOC layers. That is, the presence of hydrophobic tF8H2 SAMs protects the LMWOC layer by preventing/delaying the rinsing liquid from reaching the LMWOC layer and removing it. Upon UVO treatment, the PET surface roughens and, as a result, the quality of the SAM deteriorates. Recall that we have earlier demonstrated earlier that the thickness of the LMWOC layers increases with increasing UVO treatment time. Thicker LMWOC layers are easier to remove as the rinsing liquid can penetrate through defects present in the SAM. The highest quality SAM is obtained at very short UVO times presumably because of the interplay between the optimum hydrophilicity and thickness of the LMWOC layer and a sufficient density of tF8H2 in the SAM. In our previous work, we have established that dense tF8H2 SAMs form on substrates possessing only a moderate degree of hydrophilicity [27]. Because of the trichlorosilane functionality, the tF8H2 molecules form in-plane linkages via condensation between neighboring –OH groups (formed by hydrolysis of the chlorine atom). Interestingly, the entire sheet of cross-linked tF8H2 SAM is anchored firmly to the underlying substrate at only a few points of attachment. Presumably the same situation exists here, where only a relatively small number of –OH groups generated on PET after ≈2 min of UVO treatment is sufficient to anchor the SAM to a relatively thin LMWOC layer (*cf.* Fig. 1).

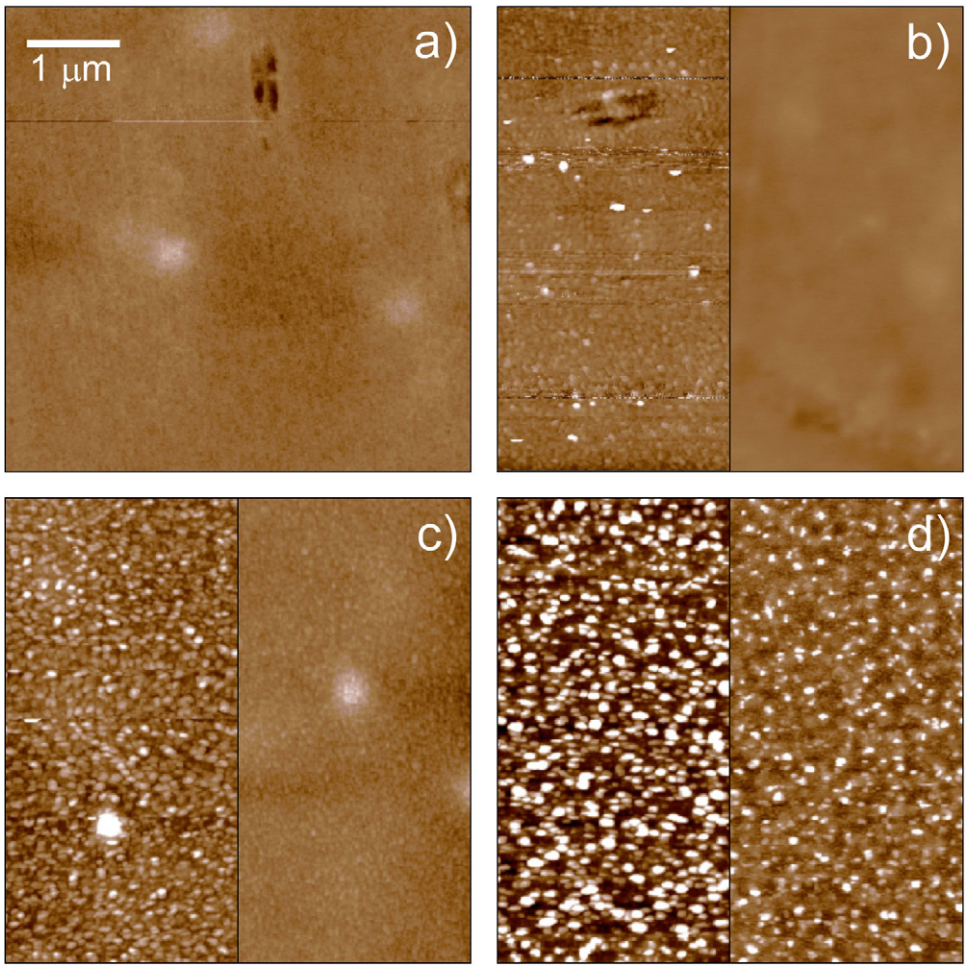

Fig. 5. AFM images of PET surfaces treated with UVO for various times (in min): (a) 0, (b) 2, (c) 8, and (d) 30. The left and right panels in parts (b)–(d) correspond to the image taken from samples before and after sonication, respectively. The height scale ranges from 0 (dark brown) to 30 nm (white). (For interpretation of the references to color in this figure legend, the reader is referred to the web version of the article.)

To provide an independent measure of this "optimal" UVO treatment time, we explore the trends present in the carbon K-edge NEXAFS spectra. Fig. 8 shows the carbon K-edge PEY NEXAFS spectra acquired at $\theta = 50^\circ$ from PET-UVO/tF8H2 samples prepared by treating PET substrates for various UVO times, followed by tF8H2 SAM deposition and washing. In all the spectra, the peak at 292 eV, which corresponds to the $1s \rightarrow \sigma^*$ transition of the C–F bond, is readily detected. While the spectra corresponding to UVO times $\leq$4 min

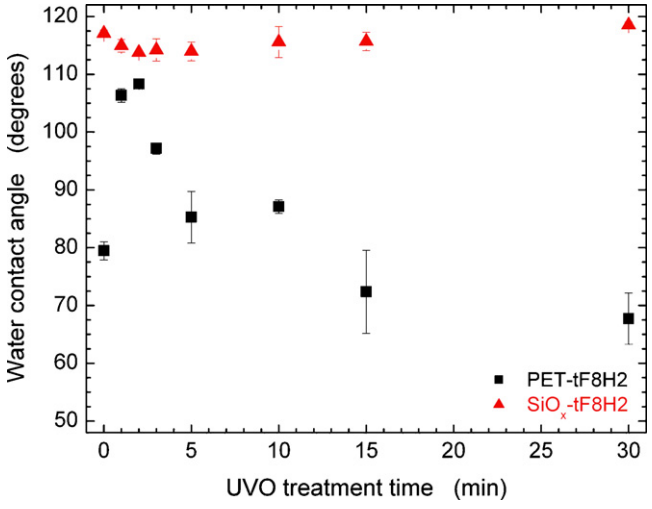

Fig. 6. Water contact angles of PET-UVO/tF8H2 (squares) and SiO_x/tF8H2 (triangles) samples as function of UVO treatment time. (For interpretation of the references to color in this figure legend, the reader is referred to the web version of the article.)

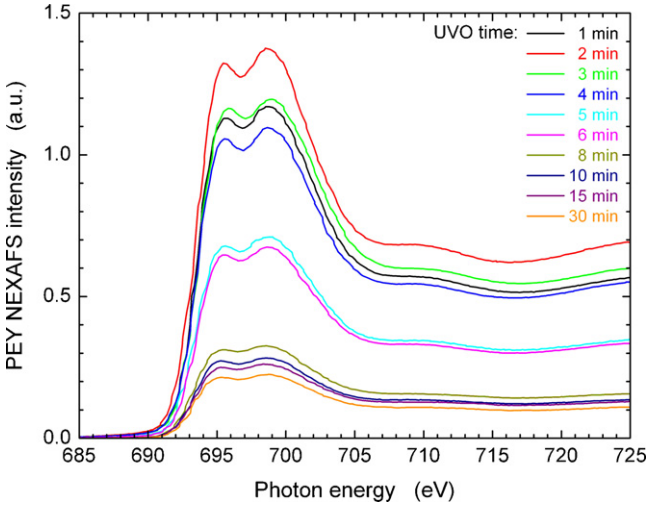

Fig. 7. Fluorine K-edge PEY NEXAFS spectra collected from PET modified with UVO for various times ranging from 1 to 30 min and covered with tF8H2 SAM. (For interpretation of the references to color in this figure legend, the reader is referred to the web version of the article.)

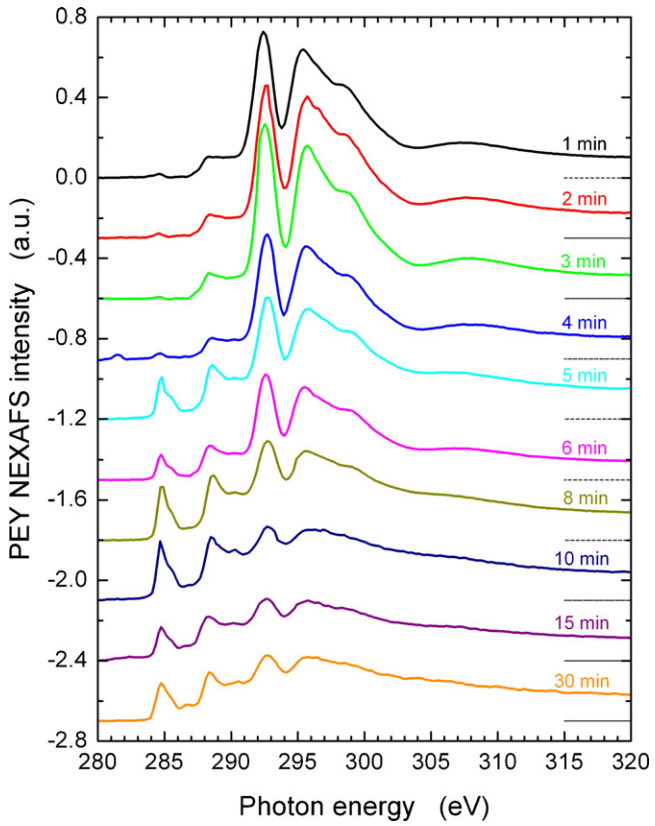

Fig. 8. Carbon K-edge PEY NEXAFS spectra collected from PET modified with UVO for various times ranging from 1 to 30 min and covered with tF8H2 SAM. The PEY NEXAFS spectra for samples treated for UVO times longer than 1 min have been shifted vertically by −0.3 (with respect to the preceding spectrum) on a relative intensity scale. The lines below each spectrum denote the PEY NEXAFS intensity corresponding to the pre-edge intensity signal for that spectrum. (For interpretation of the references to color in this figure legend, the reader is referred to the web version of the article.)

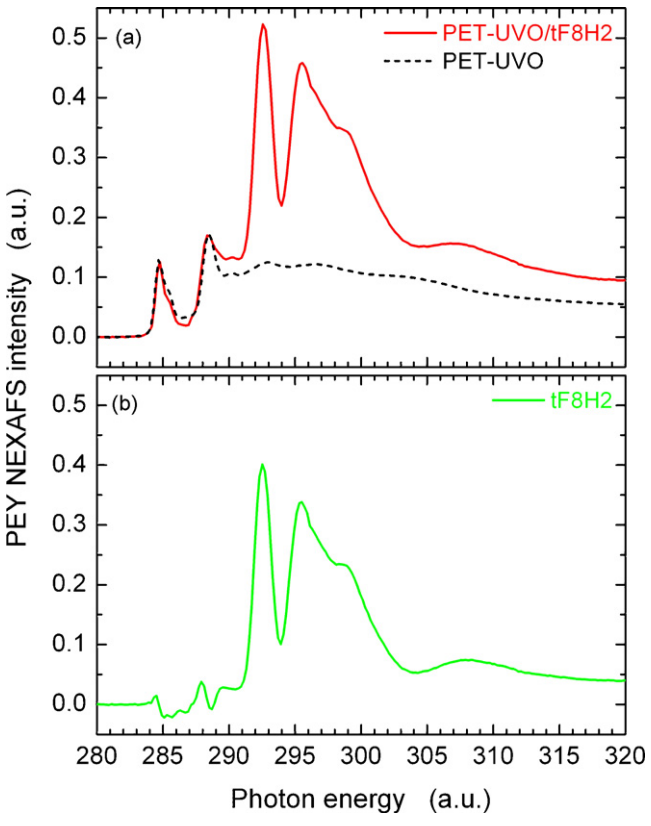

Fig. 9. (a) PEY NEXAFS spectrum from PET-UVO (black dashed line) and PET-UVO covered with tF8H2 SAM (red solid line). In both cases the UVO time was 6 min. (b) Difference PEY NEXAFS intensity obtained by subtracting the PET-UVO spectrum (dashed line in part a) from the PET-UVO/tF8H2 spectrum (solid line in part a). (For interpretation of the references to color in this figure legend, the reader is referred to the web version of the article.)

appear qualitatively similar to those measured from SiO_x/tF8H2 SAMs (data not shown), a new spectral feature appears at 285 eV in samples treated for UVO times in excess of 4 min. This peak, composed of two smaller peaks located at 284.8 and 285.3 eV, identifies the $1s \rightarrow \pi^*$ transition in the C=C signal from PET. Detection of this peak requires that PET must be present within the first ≈3–4 nm of the sample surface, a typical probing depth for the PEY NEXAFS signal, and that, by inference, an incomplete SAM is present on the sample surface. Along with the appearance of the $1s \rightarrow \pi^*_{C=C}$ signal, the intensity of the $1s \rightarrow \sigma^*_{C-F}$ peak decreases, indicating a reduced concentration of fluorine in the specimen. Quantitative comparison of the spectra shown in Fig. 8 in conjunction with the corresponding NEXAFS spectrum collected from the PET-UVO sample treated for the same UVO exposure time can yield the amount of tF8H2 present in the sample. In Fig. 9a we replot the carbon K-edge PEY NEXAFS spectrum from the PET-UVO/tF8H2 sample treated for 6 min and superimpose the spectrum measured from the PET-UVO sample treated for the same exposure time. The latter spectrum was multiplied by a scaling coefficient (K) to match the intensity of the $1s \rightarrow \pi^*_{C=C}$ peak (from 283 to 288 eV) in the PET-UVO/tF8H2 sample. Subsequent subtraction of the two spectra yields a spectrum that corresponds closely to that of a pure tF8H2 SAM, as shown in Fig. 9b. The PEY NEXAFS carbon K-edge jump intensities obtained from such difference spectra as the one shown in Fig. 9b are plotted on the left ordinate in Fig. 10. Included for completeness in Fig. 10 are the corresponding K values on the right ordinate. The edge-jump values exhibit a maximum at 2 min of UVO treatment, in agreement with our previous observations, after which time they start to decrease with increasing UVO time, eventually leveling off at ≈8–10 min. The magnitude of K can be considered as a measure of the fraction of tF8H2 SAMs removed together with the LMWOC layer upon rinsing. The K values are small at short UVO times, but increase sharply with increasing UVO treatment time after about 4 min and ultimately reach a plateau (between 0.23 and

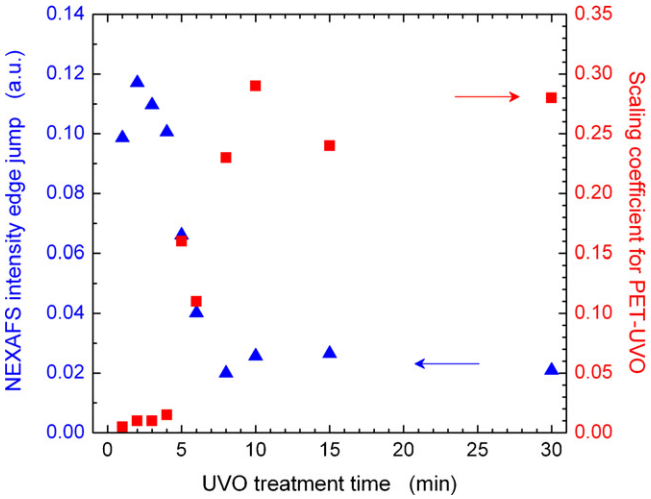

Fig. 10. Edge-jump in PEY NEXAFS intensity from difference spectra (*cf.* Fig. 9) determined at 320 eV as a function of UVO treatment time (blue triangles). Scaling coefficient (K) values as defined in the text are also included as a function of UVO treatment time (red squares). (For interpretation of the references to color in this figure legend, the reader is referred to the web version of the article.)

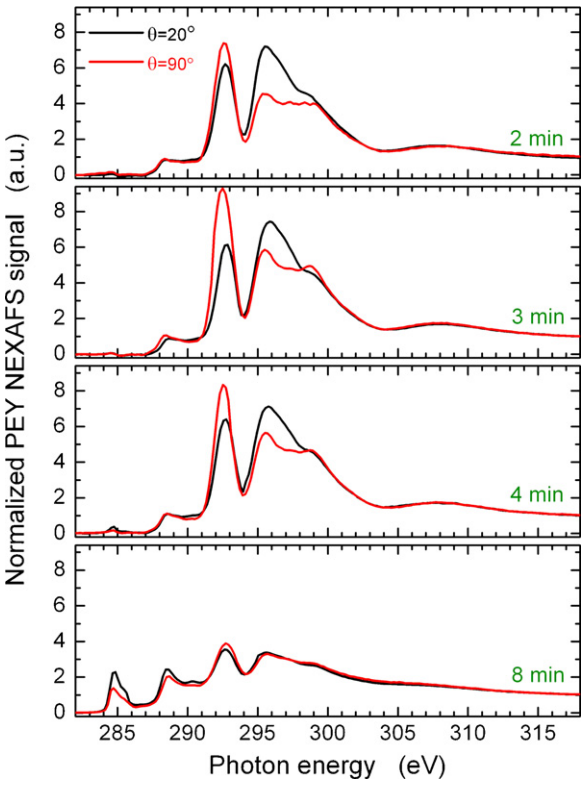

Fig. 11. Normalized PEY NEXAFS spectra collected from PET-UVO/tF8H2 specimens at the carbon K-edge in two different sample orientations θ (defined as the angle between the surface normal and the electric vector of the incident X-ray beam): 20° (black) and 90° (red). The PET was treated with UVO for various times ranging from 2 (top) to 8 (bottom) min. (For interpretation of the references to color in this figure legend, the reader is referred to the web version of the article.)

0.29) for times longer than ≈8–10 min. We recognize that, in this analysis, we have neglected small differences in the X-ray absorption cross section between PET-UVO and PET-UVO/tF8H2. While approximate, the values of K displayed in Fig. 10 provide valuable information about the coverage of the PET-UVO substrate by the SFOS SAM.

The concentration of tF8H2 molecules on the UVO-modified PET surface determines the number of generated Auger electrons, which contribute to the PEY signal. In addition, the orientation of the antibonding orbitals relative to the electric vector of the polarized X-ray beam also affects the intensity of the $1s \rightarrow \sigma^*$ transition signals. To extract information regarding the molecular concentration and orientation of SFOS molecules from NEXAFS spectroscopy, PEY NEXAFS spectra have been collected from PET-UVO/tF8H2 samples at various orientations of the samples with respect to the incident X-ray beam. In Fig. 11, normalized PEY NEXAFS spectra are presented as a function of photon energy around the carbon K-edge at $\theta = 20°$ and 90° for different UVO treatment times. The most important peaks in these spectra appear at 292 and 295 eV, corresponding to the $1s \rightarrow \sigma^*_{C-F}$ and $1s \rightarrow \sigma^*_{C-C}$ signals, respectively. By comparing the relative intensities of these two peaks at various orientations, we can infer that the tF8H2 chains are oriented nearly perpendicularly to the substrates (the peak at 292 eV is higher and that at 295 eV is lower at $\theta = 90°$ relative to the intensities collected $\theta = 20°$) [36,37]. While a quantitative measure of molecular orientation is not provided here, it suffices to say that a reasonable measure of the degree of perpendicular orientation is the difference between the spectra collected at $\theta = 20°$ and 90°. The largest difference between these peak intensities in the spectra shown in Fig. 11 is evident for the PET-UVO/tF8H2 sample treated for 3 min. At longer UVO times, the NEXAFS spectra do not exhibit any discernible tF8H2 orientation, even though the SFOS SAMs remain attached to the underlying substrate, as evidenced by the presence of the fluorine signal. The absence of orientation detected in the specimens does not, however, necessarily mean that the tF8H2 chains are not oriented in the SAMs. Due to surface roughening of the substrate, portions of the SAM may still be oriented but point in different directions. Since these regions are expectedly much smaller than the size of the probe (≈0.25 mm^2), NEXAFS, in its current configuration, is not capable of measuring the molecular orientation on such rough samples.

4. Conclusions

The surface of PET has been modified by using UVO, followed by subsequent attachment of a semifluorinated organosilane (SFOS) SAM to the underlying oxidized PET substrate. We observe that UVO modification increases the surface energy of PET by degrading some of the PET chains present on the surface. Such UVO-mediated degradation leads to the formation of small volatile species and larger organic aggregates, the latter of which remain on the PET surface in the form of a LMWOC layer. The surface energy and atomic oxygen concentration of the PET-UVO samples increases with increasing UVO treatment time up to 4–5 min, as evidenced from CA, XPS and NEXAFS measurements. Removal of the highly hydrophilic LMWOC layer causes small, but noticeable, increases in the S-CA and surface carbon content. In addition, an increase in UVO treatment time is accompanied by surface roughening, as discerned by AFM. The oxidized PET surface can be used as a substrate for depositing a hydrophobic organosilane SAM layer. The quality of the SAMs generated for different UVO treatment times has been monitored with CA and NEXAFS. The S-CA of PET-UVO/tF8H2 samples reveals that some tF8H2 SAMs are removed from the substrate along with the underlying LMWOC layer during sample wash. Complementary NEXAFS measurements confirm these observations. Specifically, the concentration of fluorine ascertained from the edge-jump in the fluorine K-edge NEXAFS spectra exhibits a maximum at a UVO exposure time of 2 min, in favorable quantitative agreement with CA results. Our data confirm that the 2 min UVO treatment time represents an optimum condition for creating stable PET-UVO/tF8H2 samples. During this brief UVO exposure, oxidation of PET is sufficiently mild so that the LMWOC layer thickness does not increase substantially. Yet, it appears to be long enough so that an adequate concentration of surface-bound –OH groups, which serve as attachment points for the SFOS SAMs, is created on top of the PET-UVO surfaces. Detailed analysis of the PEY NEXAFS spectra in samples prepared by long UVO treatment times shows that <80% of the tF8H2 SAM remains attached to the substrate after sonication, which removes the LMWOC layer and a portion of the SFOS SAM attached to it. Since the bulk properties of PET remain unaffected during UVO surface treatment and subsequent SFOS SAM attachment, the results presented here provide an enticing avenue to tough materials with patternable and functionalized surfaces that can be used in 3D device fabrication or as responsive sensors.

Acknowledgments

We thank the United Resource Recovery Corporation (URRC) for supporting this research and Dr. Ryan Fuierer from Asylum Research for his assistance with AFM measurements. The NEXAFS spectroscopy experiments were conducted at the National Synchrotron Light Source, Brookhaven National Laboratory, which is supported by the U.S. Department of Energy, Division of Materials Sciences and Division of Chemical Sciences.

References

[1] J. Scheirs, T.E. Long, Modern Polyesters: Chemistry and Technology of Polyesters and Copolyesters, John Wiley & Sons, Hoboken, NJ, 2003, p. 750.
[2] Plastic Business Data and Charts The Association of German Plastics Manufacturers http://www.vke.de, 2004.
[3] S. Roux, S. Demoustier-Champagne, Journal of Polymer Science Part A: Polymer Chemistry 9 (2003) 1347–1359.
[4] J. Dave, R. Kumar, H.C. Srivastava, Journal of Applied Polymer Science 2 (1987) 455–477.
[5] M.S. Ellison, L.D. Fisher, K.W. Alger, S.H. Zeronian, Journal of Applied Polymer Science 1 (1982) 247–257.
[6] E.M. Saunders, S.H. Zeronian, Journal of Applied Polymer Science 11 (1982) 4477–4491.
[7] W. Chen, T.J. McCarthy, Macromolecules 11 (1998) 3648–3655.
[8] L.N. Bui, M. Thompson, N.B. McKeown, A.D. Romaschin, P.G. Kalman, Analyst 5 (1993) 463–474.
[9] Y. Avny, L. Rebenfeld, Journal of Applied Polymer Science 3 (1986) 4009–4025.
[10] R. Fukai, P.H.R. Dakwa, W. Chen, Journal of Polymer Science Part A: Polymer Chemistry 21 (2004) 5389–5400.
[11] Y.L. Hsieh, E.Y. Chen, Industrial & Engineering Chemistry Product Research and Development 2 (1985) 246–252.
[12] M. Strobel, M.J. Walzak, J.M. Hill, A. Lin, E. Karbashewski, C.S. Lyons, Journal of Adhesion Science and Technology 3 (1995) 365–383.
[13] J.M. Hill, E. Karbashewski, A. Lin, M. Strobel, M.J. Walzak, Journal of Adhesion Science and Technology 12 (1995) 1575–1591.
[14] M.J. Walzak, S. Flynn, R. Foerch, J.M. Hill, E. Karbashewski, A. Lin, M. Strobel, Journal of Adhesion Science and Technology 9 (1995) 1229–1248.
[15] D.O.H. Teare, C. Ton-That, R.H. Bradley, Surface and Interface Analysis 4 (2000) 276–283.
[16] C. Ton-That, D.O.H. Teare, P.A. Campbell, R.H. Bradley, Surface Science (1999) 278–282.
[17] J.M. Pochan, L.J. Gerenser, J.F. Elman, Polymer 27 (1986) 1058–1062.
[18] M. Strobel, C.S. Lyons, J.M. Strobel, R.S. Kapaun, Journal of Adhesion Science and Technology 4 (1992) 429–443.
[19] D. Briggs, D.G. Rance, C.R. Kendall, A.R. Blythe, Polymer 19 (1980) 895–900.
[20] P. Bertrand, Y. Depuydt, J.M. Beuken, P. Lutgen, G. Feyder, Nuclear Instruments & Methods in Physics Research Section B-Beam Interactions with Materials and Atoms (1987) 887–890.
[21] E. Arenholz, J. Heitz, M. Wagner, D. Bauerle, H. Hibst, A. Hagemeyer, Applied Surface Science 1–4 (1993) 16–19.
[22] N.P. Desai, J.A. Hubbell, Biomaterials 2 (1991) 144–153.
[23] J.R. Vig, Journal of Vacuum Science & Technology A: Vacuum, Surfaces, and Films 3 (1985) 1027–1034.
[24] J. Peeling, D.T. Clark, Journal of Polymer Science Part A: Polymer Chemistry 7 (1983) 2047–2055.
[25] I. Mathieson, R.H. Bradley, International Journal of Adhesion and Adhesives 1 (1996) 29–31.
[26] L.F. MacManus, M.J. Walzak, N.S. McIntyre, Journal of Polymer Science Part A: Polymer Chemistry 14 (1999) 2489–2501.
[27] K. Efimenko, J.A. Crowe, E. Manias, D.W. Schwark, D.A. Fischer, J. Genzer, Polymer 22 (2005) 9329–9341.
[28] J. Stöhr, NEXAFS Spectroscopy, vol. 25, Springer-Verlag, Berlin; New York, 1992, p. 403.
[29] J. Peeling, G. Courval, M.S. Jazzar, Journal of Polymer Science: Polymer Chemistry Edition (1984) 419–428.
[30] D.J. Briggs, Surface Analysis of Polymers by XPS and Static SIMS, Cambridge University Press, Cambridge, U.K.; New York, 1998, p. 198.
[31] H. Windawi, F.F. Ho, Applied Electron Spectroscopy for Chemical Analysis, vol. 64, Wiley, New York, 1982, p. 213.
[32] D.W. Dwight, T.J. Fabish, H.R. Thomas, Photon, Electron, and Ion Probes of Polymer Structure and Properties, vol. 162, American Chemical Society. Division of Organic Coatings and Plastics Chemistry; American Chemical Society. Division of Polymer Chemistry, Washington, D.C., 1981, p. 442.
[33] A. Ulman, Chemical Reviews 4 (1996) 1533–1554.
[34] F. Schreiber, Progress in Surface Science 5–8 (2000) 151–256.
[35] J. Genzer, K. Efimenko, D.A. Fischer, Langmuir 24 (2002) 9307–9311.
[36] J. Genzer, E. Sivaniah, E.J. Kramer, J.G. Wang, H. Korner, M.L. Xiang, K. Char, C.K. Ober, B.M. DeKoven, R.A. Bubeck, M.K. Chaudhury, S. Sambasivan, D.A. Fischer, Macromolecules 5 (2000) 1882–1887.
[37] J. Genzer, K. Efimenko, Science 5499 (2000) 2130–2133.